

# **Towards personalised assessment of abdominal aortic aneurysm structural integrity**

Mostafa Jamshidian<sup>1</sup>, Adam Wittek<sup>1</sup>, Hozan Mufty<sup>2, 3</sup>, Geert Maleux<sup>4</sup>, Inge Fourneau<sup>2, 3</sup>, Elke R. Gizewski<sup>5</sup>, Eva Gassner<sup>5</sup>, Alexander Loizides<sup>5</sup>, Maximilian Lutz<sup>5</sup>, Florian K. Enzmann<sup>6</sup>, Donatien Le Liepvre<sup>7</sup>, Florian Bernard<sup>7</sup>, Ludovic Minvielle<sup>7</sup>, Antoine Fondanèche<sup>7</sup>, Karol Miller<sup>1,\*</sup>

<sup>1</sup> Intelligent Systems for Medicine Laboratory, The University of Western Australia, Perth, Western Australia, Australia

<sup>2</sup> Department of Vascular Surgery, University Hospitals Leuven, Leuven, Belgium

<sup>3</sup> Department of Cardiovascular Sciences, Research Unit of Vascular Surgery, KU Leuven, Leuven, Belgium

<sup>4</sup> Department of Radiology, University Hospitals Leuven, Leuven, Belgium

<sup>5</sup> Department of Radiology, Medical University of Innsbruck, Innsbruck, Austria

<sup>6</sup> Department of Vascular Surgery, Medical University of Innsbruck, Innsbruck, Austria

<sup>7</sup> Nurea, Bordeaux, France

## Abstract

Abdominal aortic aneurysm (AAA) is a life-threatening condition involving the permanent dilation of the aorta, often detected incidentally through imaging for some other condition. The standard clinical approach to managing AAA follows a one-size-fits-all model based on aneurysm size and growth rate, leading to underestimation or overestimation of rupture risk in individual patients. The widely studied stress-based rupture risk estimation using computational biomechanics requires wall strength information. However, non-invasive methods for local patient-specific wall strength measurement have not yet been developed. Recently, we introduced an image-based approach for patient-specific, in vivo, non-invasive AAA kinematic analysis using time-resolved 3D computed tomography angiography (4D-CTA) images to measure wall strain throughout the cardiac cycle. In the present study, we integrated wall tension computation and strain measurement to develop a novel measure of local structural integrity of AAA wall – Relative Structural Integrity Index (RSII), independent of material properties and thickness of the wall and conditions of blood pressure measurement. Our methods provide a visual map of AAA wall structural integrity for individual patients using only their medical images and blood pressure data. We applied our methods to twelve patients. Additionally, we compared our measure of structural integrity of aneurysmal and non-aneurysmal aortas. Our results show similar values of the wall structural integrity measure across the patients, indicating the reliability of our methods. In line with experimental observations reported in the literature, our analysis revealed that localized low stiffness areas are primarily found in the most dilated AAA regions. Our results clearly demonstrate that the AAA wall is stiffer than the non-aneurysmal aorta.

**Keywords:** Abdominal aortic aneurysm, Rupture risk, AAA disease progression, Patient-specific analysis, Biomechanics, Kinematics, Stiffness, Structural integrity

\* Corresponding author.

E-mail address: [karol.miller@uwa.edu.au](mailto:karol.miller@uwa.edu.au) (K. Miller).

## 1. Introduction

An abdominal aortic aneurysm (AAA) is a lasting and irreversible enlargement of the aorta that is typically asymptomatic, with diagnosis often occurring through incidental detection during imaging for some other condition. An untreated AAA can progressively enlarge and eventually rupture, which is fatal in most cases (NICE, 2020; Wanhainen et al., 2024).

The current approach to AAA management, which is based on the maximum diameter and growth rate, follows a one-size-fits-all approach that suggests clinical intervention when the aneurysm diameter exceeds 5.5 cm in men and 5 cm in women, or when the growth rate surpasses 1 cm per year (Wanhainen et al., 2024). The maximum diameter criterion may either underestimate or overestimate the rupture risk in individual AAA patients, as demonstrated by cases of ruptured AAAs with diameters below the critical diameter (Vorp, 2007) and stable, unruptured AAAs with diameters exceeding the critical diameter (Darling et al., 1977; NICE, 2020; Wanhainen et al., 2024). Autopsy results reveal that approximately 13% of AAAs with a maximum diameter of 5 cm or less ruptured, while 60% of those exceeding 5 cm may remain intact (Kontopodis et al., 2016). Ruptures of aneurysms smaller than 5 cm in patients under surveillance constitute avoidable disasters (most often patient dies) and are sometimes underreported.

AAA biomechanics, particularly wall stress analysis, has been widely studied as a potential tool to personalize disease management for individual patients (Chung et al., 2022; Farotto et al., 2018; Fillinger et al., 2003; Fillinger et al., 2002; Gasser et al., 2010; Gasser et al., 2022; Grassl et al., 2024; Indrakusuma et al., 2016; Joldes et al., 2016; Joldes et al., 2017; Li et al., 2008; Liddelow et al., 2023; Miller et al., 2020; Polzer et al., 2020; Singh et al., 2023; Speelman et al., 2007; Vande Geest et al., 2006; Wang et al., 2023). While biomechanical models have progressed to estimate patient-specific AAA wall tension (i.e., the stress resultant tangential to the aneurysm surface) without requiring information on the wall mechanical properties and thickness distribution (Joldes et al., 2016), stress- or tension-based rupture risk indicators rely on the assumption of the magnitude of the wall strength – the information not available for an individual patient, and usually derived from population-based data (Grassl et al., 2024; Singh et al., 2023). This is a major weakness of the current biomechanical approaches for personalized AAA rupture risk prediction and disease management, as direct non-invasive measurement of patient-specific in vivo wall strength is not feasible using currently available

methods. However, wall stiffness or compliance can potentially be estimated by combining patient-specific wall stress (or tension) and strain data.

Several studies have investigated the non-invasive, in vivo measurement of AAA wall strain using sequential images captured at different phases of the cardiac cycle, commonly known as 4D imaging (Cebull et al., 2019; Derwich et al., 2023; Jamshidian et al., 2025; Maas et al., 2024; Nagy et al., 2015; Raut et al., 2014; Satriano et al., 2015; Wang et al., 2018; Wittek et al., 2017; Wittek et al., 2018). Several studies (Nagy et al., 2015; Satriano et al., 2015) proposed that analysis of wall strain can be used to obtain patient-specific information about the aneurysm wall material properties and estimate the aneurysm wall rupture risk. Recently, we developed and validated a method for patient-specific, in vivo, and non-invasive AAA kinematic analysis by applying deformable image registration to time-resolved 3D computed tomography angiography (4D-CTA) images, enabling the measurement of wall strain throughout the cardiac cycle (Jamshidian et al., 2025). To the best of our knowledge, no attempt has been made so far to perform an in vivo structural integrity analysis of the AAA wall by directly comparing stress (or tension) and strain.

In this study, we combine the AAA wall strain measurement with the patient-specific calculation of tension within the AAA wall to formulate a novel Relative Structural Integrity Index (RSII) as a potential indicator for assessing the severity of AAA disease. We calculate the distribution of this index on the AAA surface for twelve patients, whose 4D CTA images were sourced from Fiona Stanley Hospital in Australia, University Hospitals Leuven in Belgium, and Medical University of Innsbruck in Austria. RSII takes into account both the tension in the AAA wall, computed using an established finite element (FE)-based stress recovery technique (Joldes et al., 2016; Joldes et al., 2017; Joldes et al., 2018), and the strain derived from deformable image registration of individual 3D frames of 4D-CTA image, thereby integrating wall internal force information with AAA kinematics (Jamshidian et al., 2025).

The paper is organized as follows: In Section 2, we present the image data of AAA patients and the methods for estimating wall stress, tension and strain, and then introduce our patient-specific RSII of the AAA wall. In Section 3, we present the results for AAA wall tension, strain, and RSII in twelve patients, followed by conclusions and discussion in Section 4.

## 2. Materials and methods

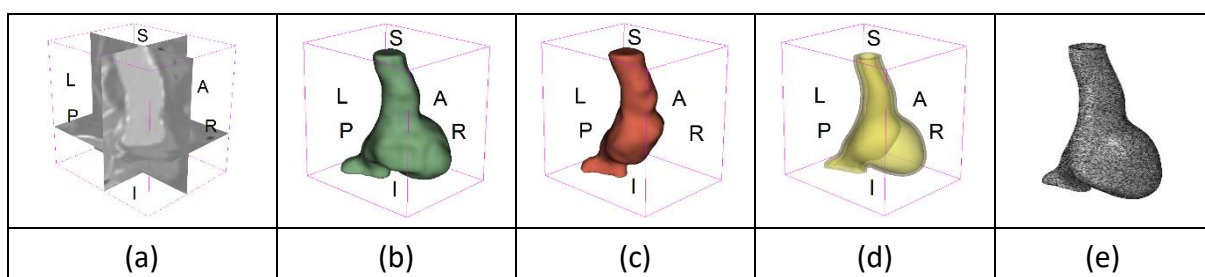
### 2.1. Image data

We used anonymized contrast-enhanced 4D-CTA image datasets from twelve AAA patients, with each dataset consisting of ten 3D volume frames per cardiac cycle. Patients 1 to 10 were recruited at Fiona Stanley Hospital (Perth, Australia), patient 11 at University Hospitals Leuven (Leuven, Belgium), and patient 12 at Medical University of Innsbruck (Innsbruck, Austria), with informed consent obtained before their participation. The study was conducted in accordance with the Declaration of Helsinki, and the protocols were approved by Human Research Ethics and Governance at South Metropolitan Health Service (HREC-SMHS) (approval code RGS3501), Human Research Ethics Office at The University of Western Australia (approval code RA/4/20/5913), Ethics Committee of University Hospitals Leuven (approval code S63163), and Ethics Committee of Medical University of Innsbruck (approval code 1271/2023). Table 1 provides the image dimensions and resolutions for each patient, as well as the maximum AAA diameter, which is currently the primary criterion for surgical intervention. The image size and resolution varied among individuals depending on the permitted safe radiation dose, which was determined by the patient's weight and height. The average age of the patients was 77 years. Of the patients, 80% were men and 20% were women, consistent with the higher prevalence of AAA in men compared to women.

As an example of the image data, Figure 1a shows the cropped 3D-CTA image of Patient 1's AAA in systolic phase. The image dimensions are 72 x 61 x 83 voxels, with voxel spacing of 1.18 mm x 1.18 mm x 1.00 mm along the R (left-right direction), A (posterior-anterior direction), S (inferior-superior direction) axes, as illustrated in Figure 1. In the patient coordinate system, the basis vectors align with the anatomical axes: anterior-posterior, inferior-superior, and left-right.

**Table 1.** Computed tomography angiography (CTA) image dimensions and resolutions for twelve patients with abdominal aortic aneurysm (AAA), along with the maximum AAA diameter for each patient. Patients 1 to 10 were from Fiona Stanley Hospital (Perth, Australia), patient 11 from University Hospitals Leuven (Leuven, Belgium), and patient 12 from Medical University of Innsbruck (Innsbruck, Austria).

Patient No.	Image dimensions (pixels)	Image resolution (mm)	AAA maximum diameter (mm)
1	256 × 256 × 254	1.18 × 1.18 × 1.00	65.8
2	512 × 512 × 169	0.63 × 0.63 × 1.50	67.2
3	512 × 512 × 143	0.63 × 0.63 × 1.00	50.9
4	256 × 256 × 177	0.81 × 0.81 × 1.50	59.3
5	256 × 256 × 482	1.82 × 1.82 × 1.00	52.7
6	256 × 256 × 488	1.53 × 1.53 × 1.00	47.1
7	512 × 512 × 160	0.63 × 0.63 × 1.00	57.3
8	512 × 512 × 155	0.31 × 0.31 × 1.00	44.2
9	256 × 256 × 170	1.25 × 1.25 × 1.00	50.2
10	256 × 256 × 184	1.25 × 1.25 × 1.00	52.3
11	512 × 512 × 171	0.31 × 0.31 × 0.70	53.2
12	512 × 512 × 137	0.23 × 0.23 × 1.00	61.4



**Figure 1.** Patient 1's abdominal aortic aneurysm (AAA): (a) Cropped 3D-CTA image, (b) AAA label map, (c) Blood label map, (d) Surface model of AAA including ILT, and (e) Finite element (FE) mesh.

## 2.2. Stress and tension

For stress and tension computations, we used BioPARR (Biomechanics-based Prediction of Aneurysm Rupture Risk), a free software package for AAA biomechanical analysis based on the FE method (<https://bioparr.mech.uwa.edu.au/>) (Joldes et al., 2017). Given the patient's blood pressure, along with the AAA and blood segmentations (label maps) extracted from medical images, BioPARR performs automated, efficient, and robust wall stress recovery using the linear FE method and integrates the tangential components of the stress tensor over the wall thickness to obtain a stress resultant – the wall tension (N/m) that, unlike stress, is independent of very difficult to measure AAA wall thickness.

This efficient methodology enables rapid computation of the wall tension that balances the applied blood pressure load (in the deformed configuration), without requiring the mechanical properties of the wall tissue nor its thickness (Ciarlet, 2021; Joldes et al., 2016; Joldes et al., 2017). Alternatively, a sophisticated non-linear inverse methodology can be applied to recover stress and tension by “unloading” an AAA (see, e.g., (Joldes et al., 2015; Lu et al., 2007, 2008; Miller and Lu, 2013)), but our experience shows that these complicated methods yield the results that are, for practical purposes, the same as those obtained using our simple stress recovery approach (Joldes et al., 2016), as predicted by the theory (Ciarlet, 2021).

To extract AAA geometry, we used PRAEVAorta by NUREA (<https://www.nurea-soft.com/>) for AI-based automatic segmentation of 3D-CTA image (see Figure 1a), followed by automated post-processing with an in-house MATLAB code (Alkhatib et al., 2024), to automatically generate the AAA and blood label maps, as shown in Figure 1b and Figure 1c, respectively. Using these label maps and the assumed wall thickness of 1.5 mm (Raut et al., 2013), we then ran BioPARR to automatically extract the wall and intraluminal thrombus (ILT) geometries, create the AAA surface model (Figure 1d), generate FE mesh, fix the top and bottom ends of the AAA, apply a uniform pressure of 13 kPa to the inner surface of the ILT, call Abaqus/Standard FE package (Simulia, 2024) to recover stress using the FE method, incorporate residual stresses using the Fung's Uniform Stress Hypothesis (Fung, 1991; Joldes et al., 2018) and finally integrate tangential components of stress (therefore “integrating out” the assumed wall thickness) to output the wall tension.

The mesh generated using BioPARR, shown in Figure 1e, consists of 824579 nodes and 481928 10-node quadratic tetrahedron elements with hybrid formulation and constant pressure (element type C3D10H in Abaqus) (Alkhatib et al., 2023). For stress recovery, BioPARR assumes isotropic linear elastic material properties for the wall tissue, with a Young's modulus of 100 GPa and a Poisson's ratio of 0.49. The ILT was assumed (somewhat arbitrarily) to be 20 times more compliant than the wall. The high stiffness preserves the shape of the observed aneurysm, ensuring that the stress distribution corresponds to the observed, loaded structure. This approach avoids a common mistake in the literature—applying pressure load to an already deformed geometry, de facto treating it as unloaded. This results in computing stress distribution in an unphysiological, excessively inflated AAA geometry.

BioPARR incorporates residual stresses based on Fung's Uniform Stress Hypothesis (Fung, 1991; Joldes et al., 2018), making it an easy post-processing step in AAA stress analysis (Joldes et al., 2018). We previously confirmed that, for a given material model and properties, the residual stress fields generated by the BioPARR method closely match those obtained through the more complex non-linear iterative stress analysis methods (Joldes et al., 2018; Polzer et al., 2013). Finally, in another post-processing step, wall tension is computed by integrating the tangential components of the stress tensor over the wall thickness, resulting in a stress resultant independent of the assumed wall thickness.

### **2.3. Strain**

To compute AAA wall displacement and strain, we applied deformable image registration to align the systolic and diastolic 3D frames of the 4D-CTA, estimating the displacement field that maps the systolic to the diastolic AAA geometry. Next, we derived wall displacements from the registration displacement field and then calculated wall strain.

We used a MATLAB implementation of deformable image registration with isotropic total variation regularization of displacement (Jamshidian et al., 2025; Vishnevskiy et al., 2017). For details on the image registration theory and algorithm, the reader may refer to our recent work on AAA kinematics (Jamshidian et al., 2025).

We interpolated the registration displacement field at the AAA wall, represented by a point cloud, to obtain the wall displacement from registration in the Cartesian patient coordinate system (R, A, S). We have previously shown that registration produces more accurate



displacements in the direction of the image gradient, which, in the case of the wall region of AAA 3D-CTA images, closely aligns with the wall normal (Jamshidian et al., 2025; Lehoucq et al., 2021). Thus, we established a local biological coordinate system consisting of the local normal and two perpendicular tangents to the wall surface using 3D plane fitting via the planar least squares regression method (Berkmann and Caelli, 1994; Shakarji, 1998) and decomposed the wall displacement into its normal  $u_n$  and tangential  $u_t$  components.

Wittek et al. (Wittek et al., 2018) used the FE method to compute the AAA wall strain field from 4D ultrasound wall motion data and demonstrated that circumferential strain is the predominant and physiologically meaningful measure of AAA wall strain. Similarly, mechanical testing of uniaxial samples harvested during open AAA repair along axial and circumferential directions revealed that wall strength in the circumferential direction is significantly higher than in the axial direction, further confirming the significance and dominance of circumferential strain (Polzer et al., 2021).

Following the methods of (Jamshidian et al., 2025; Karatolios et al., 2013; Morrison et al., 2009), we used the wall normal displacement from registration,  $u_n$ , to calculate the local circumferential wall strain as (Coelho et al., 2014; Fichter, 1997; Hencky, 1915):

$\epsilon = \frac{u_n}{R}$	(1)
----------------------------	-----

where  $R$  is the local radius of wall curvature, estimated by local surface fitting with non-deterministic outlier detection (Jamshidian et al., 2025; Torr and Zisserman, 2000).

#### 2.4. Structural Integrity Index

Attarian et al. (Attarian et al., 2019) observed longitudinal rupture lines in fully harvested ruptured AAAs and used crack propagation simulations to show that wall stress alone was unlikely to cause rupture. They concluded that rupture likely began in short segments of less than 1 cm and then propagated along the observed rupture lines.

The longitudinal rupture lines indicate the dominance of circumferential strain and wall tension in AAA rupture mechanism. Therefore, we defined a Structural Integrity Index (SII) for the AAA wall as the ratio of circumferential strain to wall tension  $t$  (N/m), i.e.,

$$SII = \frac{\epsilon}{t}$$

(2)

with units of m/N. SII serves as an indicator of the local wall compliance and offers a visual map of its variations. By quantifying the localized weakening of the wall, SII visualizes regions at risk of rupture as regions of the AAA wall with relatively high SII values compared to the surrounding regions.

As a new integrated measure of AAA wall compliance, we defined and computed the Relative Structural Integrity Index (RSII) as the SII value at a given point divided by the average absolute value of SII across the AAA wall surface, i.e.,

$$RSII = \frac{|SII|}{\text{mean}(|SII|)}$$

(3)

which may serve as a novel indicator of AAA structural soundness, the severity of AAA disease, and possibly a predictor of AAA disease progression, including rupture risk. As a relative measure, RSII is independent of blood pressure measurement accuracy. Further details on SII are provided in the Discussion section.

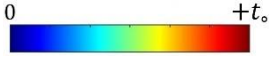
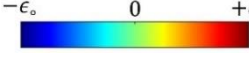

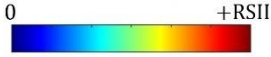
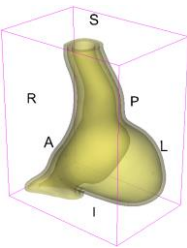
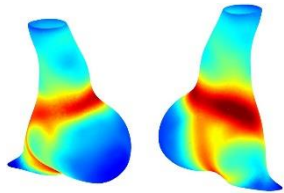
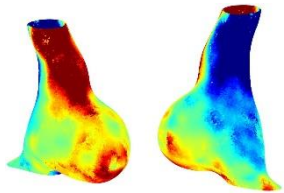
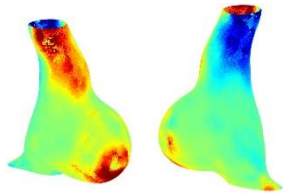
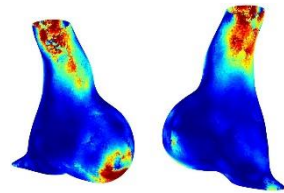
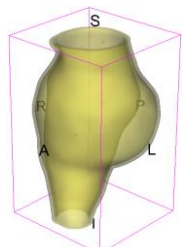
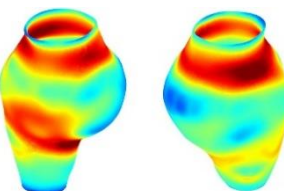
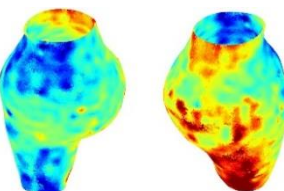
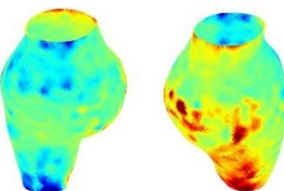
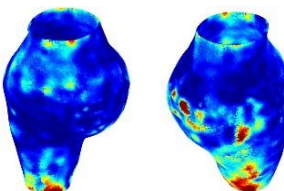
### 3. Results

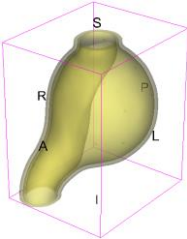
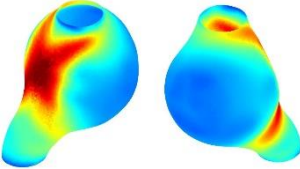
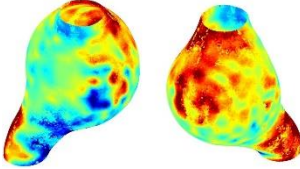
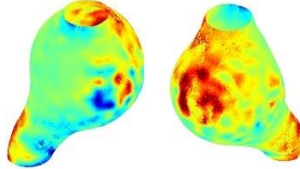
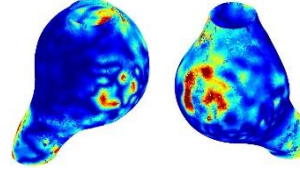
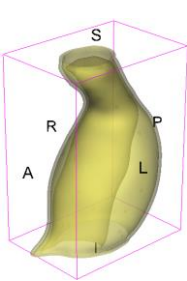
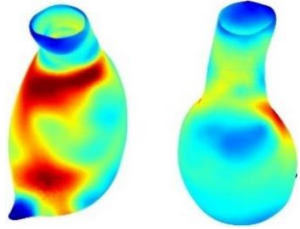
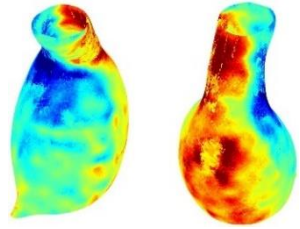
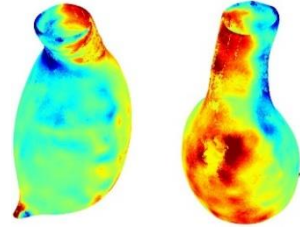
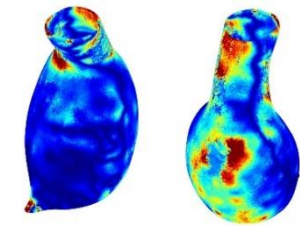
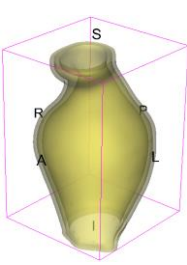
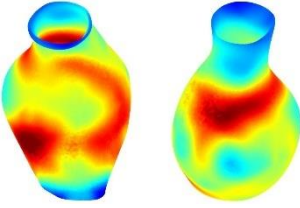
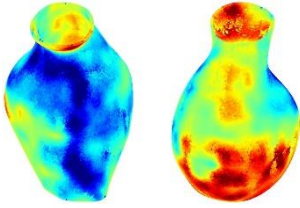
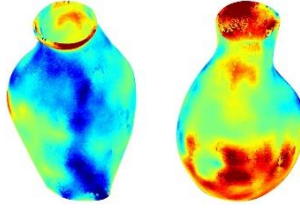
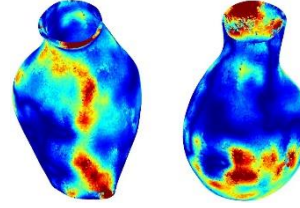
#### 3.1. AAA structural integrity

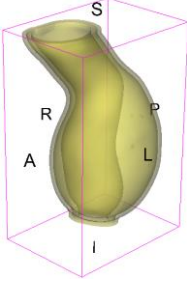
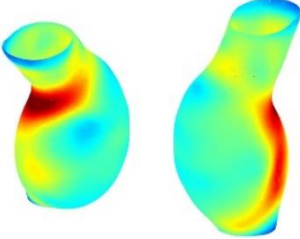
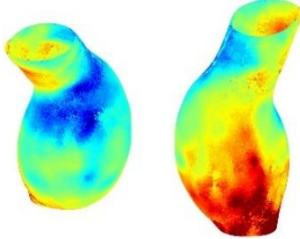
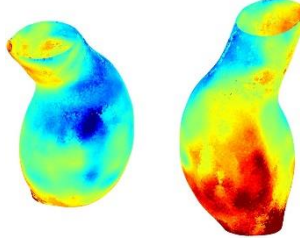
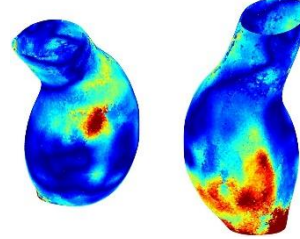
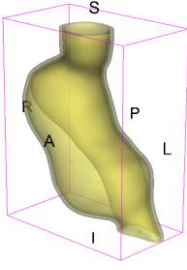
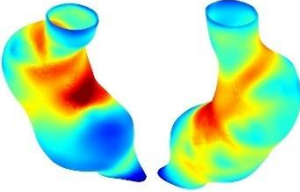
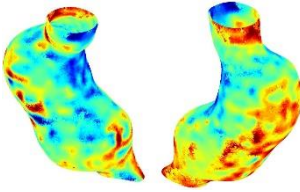
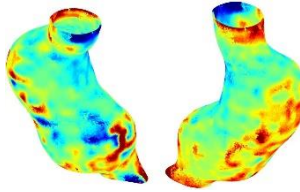
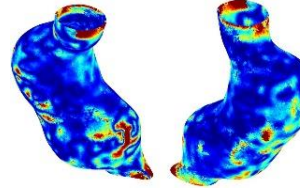
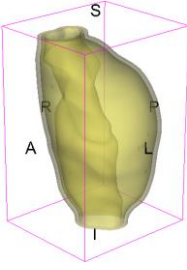
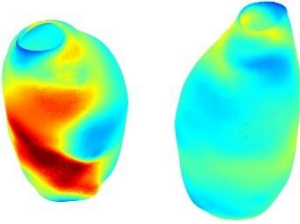
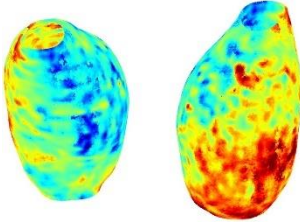
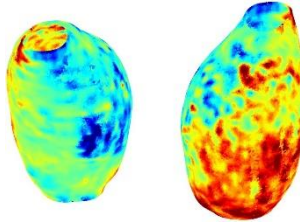
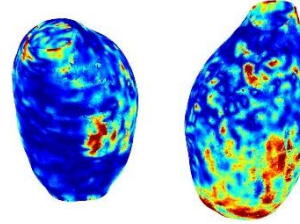
We applied our methods to evaluate AAA stress, tension, strain, and RSII in twelve patients. For each patient, we used the diastolic and systolic phases of 4D-CTA image data as the moving and fixed images in deformable image registration, respectively. For image registration parameters, see our recent work on AAA kinematics (Jamshidian et al., 2025).

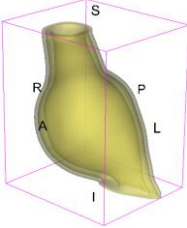
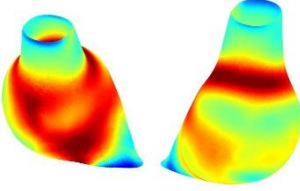
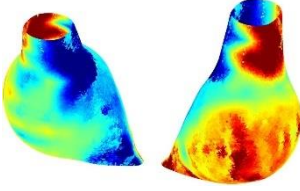
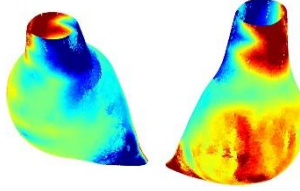
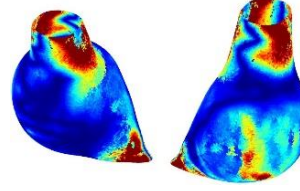
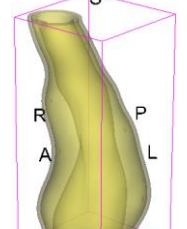
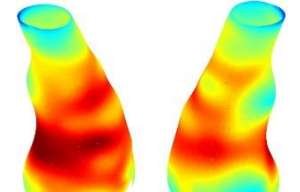
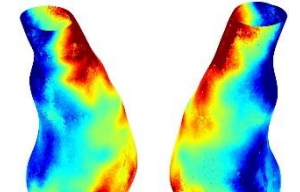
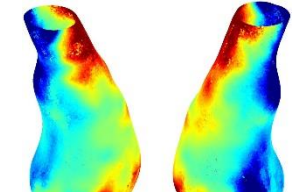
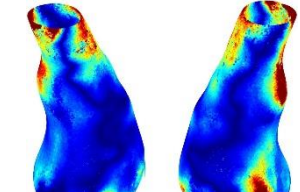
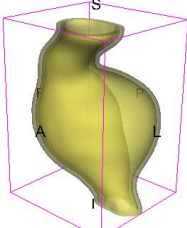
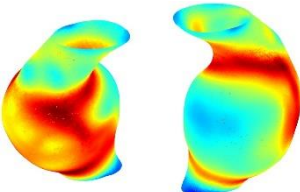
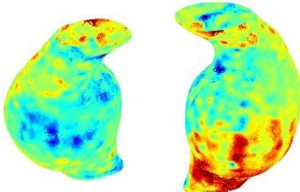
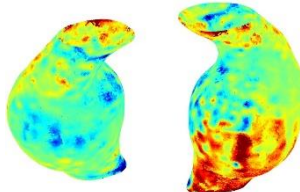
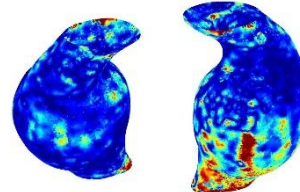
Table 2 summarizes the AAA structural integrity analysis results for twelve patients. Table 2 presents the AAA geometry and contour plots of wall tension, circumferential strain, SII and RSII for each patient, using patient-specific contour limits.

**Table 2.** AAA structural integrity analysis results for twelve patients. For each patient, the AAA geometry including ILT, and contour plots of wall tension, circumferential strain, Structural Integrity Index (SII) and Relative Structural Integrity Index (RSII) are shown. Patient-specific contour limits, including the 99th percentile wall tension  $t_o$ , the 99th percentile circumferential strain  $\epsilon_o$ , the 99th percentile structural integrity index  $SII_o$  and the 99th percentile relative structural integrity index  $RSII_o$ , are reported for each patient.

Patient number	AAA geometry including ILT	Wall tension (N/mm) 0  $+t_o$	Circumferential strain (%) $-\epsilon_o$  $+\epsilon_o$	SII (mm/N) $-SII_o$  $+SII_o$	RSII 0  $+RSII_o$
1		 $t_o = 0.27 \text{ N/mm}$	 $\epsilon_o = 4.78 \%$	 $SII_o = 1.21 \text{ mm/N}$	 $RSII_o = 4.85$
2		 $t_o = 0.44 \text{ N/mm}$	 $\epsilon_o = 5.29 \%$	 $SII_o = 0.37 \text{ mm/N}$	 $RSII_o = 4.83$

3		 <p><math>t_o = 0.29 \text{ N/mm}</math></p>	 <p><math>\epsilon_o = 5.26 \%</math></p>	 <p><math>SII_o = 0.75 \text{ mm/N}</math></p>	 <p><math>RSII_o = 4.80</math></p>
4		 <p><math>t_o = 0.38 \text{ N/mm}</math></p>	 <p><math>\epsilon_o = 4.77 \%</math></p>	 <p><math>SII_o = 0.36 \text{ mm/N}</math></p>	 <p><math>RSII_o = 3.57</math></p>
5		 <p><math>t_o = 0.38 \text{ N/mm}</math></p>	 <p><math>\epsilon_o = 4.22 \%</math></p>	 <p><math>SII_o = 0.24 \text{ mm/N}</math></p>	 <p><math>RSII_o = 3.22</math></p>

6		 <p><math>t_0 = 0.29 \text{ N/mm}</math></p>	 <p><math>\epsilon_0 = 4.98 \%</math></p>	 <p><math>SII_0 = 0.32 \text{ mm/N}</math></p>	 <p><math>RSII_0 = 3.22</math></p>
7		 <p><math>t_0 = 0.38 \text{ N/mm}</math></p>	 <p><math>\epsilon_0 = 5.94 \%</math></p>	 <p><math>SII_0 = 0.39 \text{ mm/N}</math></p>	 <p><math>RSII_0 = 3.66</math></p>
8		 <p><math>t_0 = 0.28 \text{ N/mm}</math></p>	 <p><math>\epsilon_0 = 4.56 \%</math></p>	 <p><math>SII_0 = 0.35 \text{ mm/N}</math></p>	 <p><math>RSII_0 = 3.32</math></p>

9		 <p><math>t_o = 0.29 \text{ N/mm}</math></p>	 <p><math>\epsilon_o = 2.88 \%</math></p>	 <p><math>SII_o = 0.20 \text{ mm/N}</math></p>	 <p><math>RSII_o = 3.08</math></p>
10		 <p><math>t_o = 0.25 \text{ N/mm}</math></p>	 <p><math>\epsilon_o = 4.29 \%</math></p>	 <p><math>SII_o = 0.35 \text{ mm/N}</math></p>	 <p><math>RSII_o = 3.47</math></p>
11		 <p><math>t_o = 0.26 \text{ N/mm}</math></p>	 <p><math>\epsilon_o = 9.39 \%</math></p>	 <p><math>SII_o = 0.65 \text{ mm/N}</math></p>	 <p><math>RSII_o = 4.48</math></p>

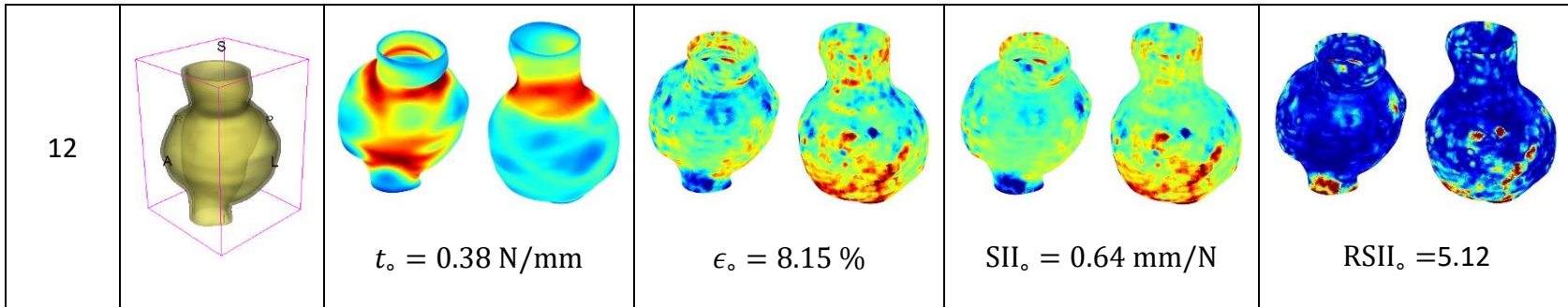


Table 2 shows that the tension and strain maps for each patient do not correlate, as high-stress regions do not align with high-strain regions, and vice versa, suggesting that pure stress-based and pure strain-based rupture risk estimations do not agree. Table 2 shows that, among all patients, the 99th percentile tension varied from 0.25 N/mm to 0.44 N/mm, with an average of 0.32 N/mm and a standard deviation of 0.06 N/mm, while the 99th percentile circumferential strain ranged from 2.88% to 9.39%, with an average of 5.38% and a standard deviation of 1.77%. For a detailed discussion on stress and strain in AAA, readers may refer to our earlier works (Jamshidian et al., 2025; Miller et al., 2020; Wittek et al., 2022).

The SII maps in Table 2 reveal a non-uniform distribution of wall compliance (i.e. the inverse of stiffness). Localized islands with high absolute SII values may indicate areas of local wall weakening, potentially increasing the likelihood of rupture in these regions. Conversely, regions with low absolute SII values suggest increased wall stiffness (or decreased wall compliance), likely due to local wall strengthening and possibly the presence of calcifications. Positive SII values represent wall compliance calculated based on positive (tensile) strain, while negative SII values indicate wall compliance calculated from negative (compressive) strain.

The RSII maps in Table 2 highlight the high-RSII regions on the AAA surface as potentially rupture-prone locations. In most AAAs, high-RSII regions, surrounded by lower RSII regions, are in the most dilated region of the AAA, which may indicate a higher likelihood of rupture in these regions. In some AAAs, such as those of patients 5, 6 and 8, high-RSII regions are also visible outside the most dilated region of the AAA. This is consistent with experiments on AAAs harvested during autopsy and inflated to rupture, which revealed that one-fourth of the specimens did not rupture in their most dilated region (Gomes et al., 2021). Additionally, more uniform and expanded high-RSII regions are identifiable outside the AAA region, towards the non-aneurysmal healthy aorta. A discussion on RSII in the non-aneurysmal aorta is provided in the next Section.

### **3.2. Healthy aorta structural integrity**

Uniaxial tensile testing of AAA wall tissue obtained during autopsy or surgery has established that AAAs are stiffer than non-aneurysmal aortas due to a decreased elastin-to-collagen ratio (He and Roach, 1994). Similarly, recent experiments on AAAs, harvested during autopsy and

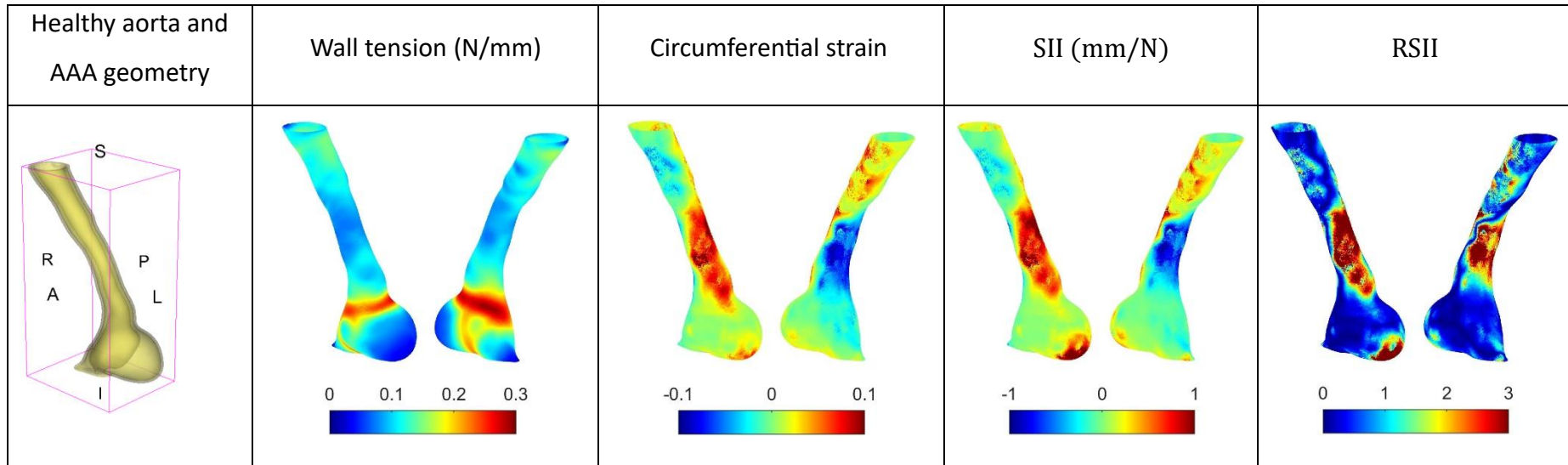


inflated to rupture, have shown that normal aortas are more compliant than AAAs (Gomes et al., 2021).

To compare RSII in the AAA with that in the healthy portions of the aorta, we performed a structural integrity analysis for Patient 1 using uncropped images that included the healthy proximal sections of the aorta above the AAA region, as shown in Table 3. The contour plots of wall tension and circumferential strain in Table 3 demonstrate that, as discussed in our previous works (Jamshidian et al., 2025; Miller et al., 2020; Wittek et al., 2022), AAA wall strains are significantly lower than those of a healthy aorta, while higher stresses are developed in the AAA region, compared to the healthy aorta, due to its inflated geometry.

The SII contour plots in Table 3 reveal regions with high absolute SII values in both the aneurysmal aorta and, notably, the non-aneurysmal aorta. The RSII contour plots in Table 3 reveal a more uniform RSII distribution in the healthy aorta proximal to the AAA compared to the AAA itself. Additionally, the non-aneurysmal aorta generally exhibits higher RSII values, reflecting higher compliance (or lower stiffness) compared to the aneurysmal aorta. This is consistent with the experimental findings reported in the literature (Gomes et al., 2021; He and Roach, 1994).

**Table 3.** Structural integrity analysis of healthy aorta for Patient 1. The AAA and healthy aorta geometry, and contour plots of wall tension, circumferential strain, Structural Integrity Index (SII) and Relative Structural Integrity Index (RSII) are presented.



#### 4. Conclusions

We proposed a novel measure of AAA wall structural integrity, the Relative Structural Integrity Index (RSII), by integrating computational biomechanics for AAA wall stress recovery with computational image-based kinematics. We calculated the Structural Integrity Index (SII) across the AAA wall as the ratio of circumferential strain to wall tension and defined the RSII as the ratio of the absolute value of SII at a given point to the average absolute value of SII across the AAA wall.

For stress computations using patient-specific image-based FE models, we used the automated pipeline in BioPARR (Biomechanics-Based Prediction of Aneurysm Rupture Risk) software package (Joldes et al., 2017). BioPARR takes the patient's blood pressure along with AAA and blood label maps segmented from medical images, recovers the stress in the AAA wall, and, in the post-processing stage, corrects the recovered stresses to incorporate the effect of residual stresses and computes wall tension. The resulting wall tension does not depend on the assumed properties of the wall tissue, nor the assumed wall thickness used in the calculations.

For strain computations from the patient's 4D-CTA images, we used a MATLAB implementation of deformable image registration with isotropic total variation regularization of displacement (Vishnevskiy et al., 2017). This approach first computes wall displacement from registration and then calculates the circumferential strain as the ratio of normal (to the AAA surface) displacement to the local radius of curvature.

We applied our methods to evaluate wall stress, tension, strain, and RSII in twelve AAAs. We also compared RSII between AAA and the non-aneurysmal aorta. In line with the published experimental observations (Gomes et al., 2021; He and Roach, 1994), our RSII maps revealed the following:

- In most AAAs, localized high-RSII islands (i.e., regions of high strain and low tension) surrounded by lower RSII regions, are identifiable in the most dilated region of the AAA, potentially indicating rupture-prone areas of local wall weakening.
- In some AAAs, high-RSII regions are also visible outside the most dilated region.
- In all AAAs, low-RSII regions in the inflated areas suggest increased wall stiffness, possibly due to the presence of calcifications.

- The more uniform high-RSII distribution in the healthy aorta, compared to the AAA wall, indicates that the healthy aorta is more compliant than the AAA wall.

Given its agreement with experimental findings, RSII has the potential to be used for non-invasive in vivo estimation of AAA disease progression, possibly including rupture risk, in individual patients. RSII addresses the key challenges of patient-specific biomechanical analysis through its two key properties: bypassing the need for patient-specific AAA wall mechanical properties and thickness, as well as precise blood pressure measurement.

RSII is independent of material properties because stress recovery in the known, deformed configuration is a linear problem that is insensitive to the properties of the continuum under consideration (Ciarlet, 2021), as demonstrated for the case of AAA, e.g., in (Joldes et al., 2016).

RSII is independent of the difficult-to-measure AAA wall thickness because, instead of stress, it uses wall tension—a stress resultant calculated from the stress tensor by "integrating the thickness out".

RSII is independent of pressure measurement conditions because it is a relative measure. As a result, any variations in blood pressure and its fluctuations over the cardiac cycle, which may proportionally affect wall tension and SII, are automatically compensated for when computing RSII.

Despite its advantages, our method has certain limitations that should be acknowledged. In current clinical practice, 4D-CTA is not commonly used for AAA diagnosis and treatment. However, given its widespread application in cardiology, it holds strong potential for integration into vascular disease management. Further work is required to properly interpret RSII distribution over the AAA surface and perhaps suggest a single numerical indicator with predictive power.

To investigate the utility of RSII in AAA disease progression and rupture risk estimation, future longitudinal cohort studies of AAA patients under surveillance should examine the correlation between RSII-based AAA assessment and clinically observed disease progression.

## Acknowledgements

This work was supported by the Australian National Health and Medical Research Council NHMRC Ideas grant No. APP2001689. Contributions of Christopher Wood and Jane Polce, radiology technicians at the Medical Imaging Department, Fiona Stanley Hospital (Murdoch, Western Australia) to patient image acquisition at Fiona Stanley Hospital, and Dr Farah Alkhatib's (The University of Western Australia) assistance in the acquisition of these images are gratefully acknowledged.

## References

- Alkhatib, F., Jamshidian, M., Liepvre, D.L., Bernard, F., Minvielle, L., Fondanèche, A., Gizewski, E., Gassner, E., Loizides, A., Lutz, M., Enzmann, F., Mufty, H., Fourneau, I., Wittek, A., Miller, K., 2024. Towards Full Automation of Geometry Extraction for Biomechanical Analysis of Abdominal Aortic Aneurysm; Neural Network-Based versus Classical Methodologies. arXiv preprint arXiv:2403.07238v2.
- Alkhatib, F., Wittek, A., Zwick, B.F., Bourantas, G.C., Miller, K., 2023. Computation for biomechanical analysis of aortic aneurysms: the importance of computational grid. *Comput Method Biomec*, 1-17.
- Attarian, S., Xiao, S., Chung, T.C., da Silva, E.S., Raghavan, M.L., 2019. Investigation of the observed rupture lines in abdominal aortic aneurysms using crack propagation simulations. *Journal of biomechanical engineering* 141, 071004.
- Berkmann, J., Caelli, T., 1994. Computation of Surface Geometry and Segmentation Using Covariance Techniques. *IEEE T Pattern Anal* 16, 1114-1116.
- Cebull, H.L., Soepriatna, A.H., Boyle, J.J., Rothenberger, S.M., Goergen, C.J., 2019. Strain Mapping From Four-Dimensional Ultrasound Reveals Complex Remodeling in Dissecting Murine Abdominal Aortic Aneurysms. *J Biomech Eng-T Asme* 141, 060907.
- Chung, T.K., Liang, N.L., Vorp, D.A., 2022. Artificial intelligence framework to predict wall stress in abdominal aortic aneurysm. *Appl Eng Sci* 10, 100104.
- Ciarlet, P.G., 2021. *Mathematical elasticity: Three-dimensional elasticity*. SIAM.
- Coelho, M., Roehl, D., Bletzinger, K.U., 2014. Numerical and analytical solutions with finite strains for circular inflated membranes considering pressure-volume coupling. *Int J Mech Sci* 82, 122-130.
- Darling, R., Messina, C., Brewster, D., Ottinger, L., 1977. Autopsy Study of Unoperated Abdominal Aortic Aneurysms. The Case for Early Resection. *Circulation* 56, 1161-164.
- Derwich, W., Keller, T., Filmann, N., Schmitz-Rixen, T., Blasé, C., Oikonomou, K., Wittek, A., 2023. Changes in Aortic Diameter and Wall Strain in Progressing Abdominal Aortic Aneurysms. *J Ultras Med* 42, 1737-1746.

Farotto, D., Segers, P., Meuris, B., Sloten, J.V., Famaey, N., 2018. The role of biomechanics in aortic aneurysm management: requirements, open problems and future prospects. *J Mech Behav Biomed* 77, 295-307.

Fichter, W.B., 1997. Some solutions for the large deflections of uniformly loaded circular membranes (NASA Technical Paper 3658).

Fillinger, M.F., Marra, S.P., Raghavan, M.L., Kennedy, F.E., 2003. Prediction of Rupture Risk in Abdominal Aortic Aneurysm during Observation: Wall Stress versus Diameter. *Journal of Vascular Surgery* 37, 724-732.

Fillinger, M.F., Raghavan, M.L., Marra, S.P., Cronenwett, J.L., Kennedy, F.E., 2002. In vivo Analysis of Mechanical Wall Stress and Abdominal Aortic Aneurysm Rupture Risk. *Journal of Vascular Surgery* 36, 589-597.

Fung, Y.C., 1991. What Are the Residual-Stresses Doing in Our Blood-Vessels. *Annals of Biomedical Engineering* 19, 237-249.

Gasser, T.C., Auer, M., Labruto, F., Swedenborg, J., Roy, J., 2010. Biomechanical Rupture Risk Assessment of Abdominal Aortic Aneurysms: Model Complexity versus Predictability of Finite Element Simulations. *European Journal of Vascular and Endovascular Surgery* 40, 176-185.

Gasser, T.C., Miller, C., Polzer, S., Roy, J., 2022. A quarter of a century biomechanical rupture risk assessment of abdominal aortic aneurysms. Achievements, clinical relevance, and ongoing developments. *Int J Numer Meth Bio* 39, e3587.

Gomes, V.C., Raghavan, M.L., da Silva, L.F.F., Gomes, J., Silvestre, G.C., Queiroz, A., Marques, M.A., Zyngier, S.P., Chung, T.K.-J., da Silva, E.S., 2021. Experimental study of rupture pressure and elasticity of abdominal aortic aneurysms found at autopsy. *Annals of vascular surgery* 70, 517-527.

Grassl, K., Gasser, T.C., Enzmann, F.K., Gratl, A., Klocker, J., Wippel, D., Walcher, D.C., Gizewski, E.R., Wipper, S.H., 2024. Early Prediction of Abdominal Aortic Aneurysm Rupture Risk Using Numerical Biomechanical Analysis. *Diagnostics* 15, 25.

He, C.M., Roach, M.R., 1994. The composition and mechanical properties of abdominal aortic aneurysms. *Journal of vascular surgery* 20, 6-13.

Hencky, H., 1915. Über den Spannungszustand in kreisrunden Platten mit verschwindender Biegesteifigkeit. *Zeitschrift Für Mathematik und Physik* 63, 311-317.

Indrakusuma, R., Jalalzadeh, H., Planken, R.N., Marquering, H.A., Legemate, D.A., Koelemay, M.J.W., Balm, R., 2016. Biomechanical Imaging Markers as Predictors of Abdominal Aortic Aneurysm Growth or Rupture: A Systematic Review. *European Journal of Vascular and Endovascular Surgery* 52, 475-486.

Jamshidian, M., Wittek, A., Sekhvat, S., Miller, K., 2025. Kinematics of abdominal aortic Aneurysms. *J Biomech* 179, 112484.

Joldes, G.R., Miller, K., Wittek, A., Doyle, B., 2016. A simple, effective and clinically applicable method to compute abdominal aortic aneurysm wall stress. *J Mech Behav Biomed* 58, 139-148.

Joldes, G.R., Miller, K., Wittek, A., Forsythe, R.O., Newby, D.E., Doyle, B.J., 2017. BioPARR: A software system for estimating the rupture potential index for abdominal aortic aneurysms. *Scientific Reports* 7, 4641.

- Joldes, G.R., Noble, C., Polzer, S., Taylor, Z.A., Wittek, A., Miller, K., 2018. A Simple Method of Incorporating the Effect of the Uniform Stress Hypothesis in Arterial Wall Stress Computations. *Acta of Bioengineering and Biomechanics* 20, 59-67.
- Joldes, G.R., Wittek, A., Miller, K., 2015. A Total Lagrangian based method for recovering the undeformed configuration in finite elasticity. *Applied Mathematical Modelling* 39, 3913-3923.
- Karatolios, K., Wittek, A., Nwe, T.H., Bihari, P., Shelke, A., Josef, D., Schmitz-Rixen, T., Geks, J., Maisch, B., Blase, C., Moosdorf, R., Vogt, S., 2013. Method for Aortic Wall Strain Measurement With Three-Dimensional Ultrasound Speckle Tracking and Fitted Finite Element Analysis. *Ann Thorac Surg* 96, 1664-1671.
- Kontopodis, N., Pantidis, D., Dedes, A., Daskalakis, N., Ioannou, C.V., 2016. The - Not So - Solid 5.5 cm Threshold for Abdominal Aortic Aneurysm Repair: Facts, Misinterpretations, and Future Directions. *Front Surg* 3, 1.
- Lehoucq, R.B., Reu, P.L., Turner, D.Z., 2021. The Effect of the Ill-posed Problem on Quantitative Error Assessment in Digital Image Correlation. *Exp Mech* 61, 609-621.
- Li, Z.Y., U-Ying-Im, J., Tang, T.Y., Soh, E., See, T.C., Gillard, J.H., 2008. Impact of calcification and intraluminal thrombus on the computed wall stresses of abdominal aortic aneurysm. *Journal of Vascular Surgery* 47, 928-935.
- Liddelow, M., Alkhatib, F., Wittek, A., Miller, K., 2023. The Effects of the Spine on the Analysis of Peak Wall Stress in Abdominal Aortic Aneurysms, in: Nash, M.P., Wittek, A., Nielsen, P.M.F., Kobielarz, M., Babu, A.R., Miller, K. (Eds.), *Computational Biomechanics for Medicine - Towards Automation and Robustness of Computations in the Clinic*. Springer International Publishing, Singapore.
- Lu, J., Zhou, X., Raghavan, M.L., 2007. Inverse elastostatic stress analysis in pre-deformed biological structures: demonstration using abdominal aortic aneurysms. *J Biomech* 40, 693-696.
- Lu, J., Zhou, X., Raghavan, M.L., 2008. Inverse method of stress analysis for cerebral aneurysms. *Biomechanics and modeling in mechanobiology* 7, 477-486.
- Maas, E.J., Donkers, K.M., de Hoop, H., Nievergeld, A.H., Thirugnanasambandam, M., van Sambeek, M.R., Lopata, R.G., 2024. In vivo Multi-perspective 3D+ t Ultrasound Imaging and Motion Estimation of Abdominal Aortic Aneurysms. *Ultrasonic Imaging*.
- Miller, K., Lu, J., 2013. On the prospect of patient-specific biomechanics without patient-specific properties of tissues. *J Mech Behav Biomed* 27, 154-166.
- Miller, K., Mufty, H., Catlin, A., Rogers, C., Saunders, B., Sciarrone, R., Fourneau, I., Meuris, B., Tavner, A., Joldes, G.R., Wittek, A., 2020. Is There a Relationship Between Stress in Walls of Abdominal Aortic Aneurysm and Symptoms? *J Surg Res* 252, 37-46.
- Morrison, T.M., Choi, G., Zarins, C.K., Taylor, C.A., 2009. Circumferential and longitudinal cyclic strain of the human thoracic aorta: age-related changes. *Journal of Vascular Surgery* 49, 1029-1036.
- Nagy, R., Csobay-Novák, C., Lovas, A., Sótonyi, P., Bojtár, I., 2015. Non-invasive time-dependent strain measurement method in human abdominal aortic aneurysms: Towards a novel approach to rupture risk estimation. *J Biomech* 48, 1876-1886.

NICE, 2020. Abdominal Aortic Aneurysm: Diagnosis and Management (NICE guideline NG156). National Institute for Health and Care Excellence

Polzer, S., Bursa, J., Gasser, T.C., Staffa, R., Vlachovsky, R., 2013. A numerical implementation to predict residual strains from the homogeneous stress hypothesis with application to abdominal aortic aneurysms. *Annals of biomedical engineering* 41, 1516-1527.

Polzer, S., Gasser, T.C., Vlachovsky, R., Kubíček, L., Lambert, L., Man, V., Novák, K., Slazansky, M., Bursa, J., Staffa, R., 2020. Biomechanical indices are more sensitive than diameter in predicting rupture of asymptomatic abdominal aortic aneurysms. *Journal of Vascular Surgery* 71, 617-626.

Polzer, S., Man, V., Vlachovský, R., Kubíček, L., Kracík, J., Staffa, R., Novotný, T., Burša, J., Raghavan, M.L., 2021. Failure properties of abdominal aortic aneurysm tissue are orientation dependent. *J Mech Behav Biomed* 114, 104181.

Raut, S.S., Jana, A., De Oliveira, V., Muluk, S.C., Finol, E.A., 2013. The Importance of Patient-Specific Regionally Varying Wall Thickness in Abdominal Aortic Aneurysm Biomechanics. *Journal of Biomechanical Engineering* 135, 081010.

Raut, S.S., Jana, A., Muluk, S.C., Doyle, M., Biederman, R.W., Finol, E.A., 2014. Estimation of Patient-Specific 3d in Vivo Abdominal Aortic Aneurysm Strain. *Proceedings of the ASME Summer Bioengineering Conference - 2013, Pt B*.

Satriano, A., Rivolo, S., Martufi, G., Finol, E.A., Di Martino, E.S., 2015. In vivo strain assessment of the abdominal aortic aneurysm. *J Biomech* 48, 354-360.

Shakarji, C.M., 1998. Least-squares fitting algorithms of the NIST algorithm testing system. *J Res Natl Inst Stan* 103, 633-641.

Simulia, 2024. Abaqus: Finite Element Analysis for Mechanical Engineering and Civil Engineering.

Singh, T.P., Moxon, J.V., Gasser, T.C., Jenkins, J., Bourke, M., Bourke, B., Golledge, J., 2023. Association between aortic peak wall stress and rupture index with abdominal aortic aneurysm-related events. *Eur Radiol* 33, 5698-5706.

Speelman, L., Bohra, A., Bosboom, E.M.H., Schurink, G.W.H., van de Vosse, F.N., Makaorun, M.S., Vorp, D.A., 2007. Effects of wall calcifications in patient-specific wall stress analyses of abdominal aortic aneurysms. *J Biomech Eng-T Asme* 129, 105-109.

Torr, P.H.S., Zisserman, A., 2000. MLESAC: A new robust estimator with application to estimating image geometry. *Comput Vis Image Und* 78, 138-156.

Vande Geest, J., Di Martino, E., Bohra, A., Makaroun, M.S., Vorp, D.A., 2006. A Biomechanics-Based Rupture Potential Index for Abdominal Aortic Aneurysm Risk Assessment: Demonstrative Application. *Annals of the New York Academy of Sciences* 1085, 11-21.

Vishnevskiy, V., Gass, T., Szekely, G., Tanner, C., Goksel, O., 2017. Isotropic Total Variation Regularization of Displacements in Parametric Image Registration. *Ieee T Med Imaging* 36, 385-395.

Vorp, D.A., 2007. Biomechanics of abdominal aortic aneurysm. *J Biomech* 40, 1887-1902.

Wang, X.C., Carpenter, H.J., Ghayesh, M.H., Kotousov, A., Zander, A.C., Amabili, M., Psaltis, P.J., 2023. A review on the biomechanical behaviour of the aorta. *J Mech Behav Biomed* 144, 105922.



Wang, Y.F., Joannic, D., Juillion, P., Monnet, A., Delassus, P., Lalande, A., Fontaine, J.F., 2018. Validation of the Strain Assessment of a Phantom of Abdominal Aortic Aneurysm: Comparison of Results Obtained From Magnetic Resonance Imaging and Stereovision Measurements. *J Biomech Eng-T Asme* 140, 031001.

Wanhainen, A., Van Herzele, I., Bastos Goncalves, F., Bellmunt Montoya, S., Berard, X., Boyle, J.R., D'Oria, M., Prendes, C.F., Karkos, C.D., Kazimierczak, A., Koelemay, M.J.W., Kölbel, T., Mani, K., Melissano, G., Powell, J.T., Trimarchi, S., Tsilimparis, N., Antoniou, G.A., Björck, M., Coscas, R., Dias, N.V., Kolh, P., Lepidi, S., Mees, B.M.E., Resch, T.A., Ricco, J.B., Tulamo, R., Twine, C.P., Branzan, D., Cheng, S.W.K., Dalman, R.L., Dick, F., Gollidge, J., Haulon, S., van Herwaarden, J.A., Ilic, N.S., Jawien, A., Mastracci, T.M., Oderich, G.S., Verzini, F., Yeung, K.K., 2024. Editor's Choice -- European Society for Vascular Surgery (ESVS) 2024 Clinical Practice Guidelines on the Management of Abdominal Aorto-Iliac Artery Aneurysms. *Eur J Vasc Endovasc Surg* 67, 192-331.

Wittek, A., Alkhatib, F., Vitásek, R., Polzer, S., Miller, K., 2022. On stress in abdominal aortic aneurysm: Linear versus non-linear analysis and aneurysm rupture risk. *Int J Numer Meth Bio* 38, e3554.

Wittek, A., Blase, C., Derwich, W., Schmitz-Rixen, T., Fritzen, C.P., 2017. Characterization of the mechanical behaviour and pathophysiological state of abdominal aortic aneurysms based on 4D ultrasound strain imaging. *Proc Spie* 10333, 7-23.

Wittek, A., Derwich, W., Fritzen, C.P., Schmitz-Rixen, T., Blase, C., 2018. Towards non-invasive in vivo characterization of the pathophysiological state and mechanical wall strength of the individual human AAA wall based on 4D ultrasound measurements. *Zamm-Z Angew Math Me* 98, 2275-2294.